Early and Late Stage Phase Separation Dynamics of Polystyrene/Poly(methyl methacrylate-*stat*-cyclohexyl methacrylate) Blends

Volker Edel

Max-Planck-Institut für Polymerforschung, Postfach 3148, 55021 Mainz, Germany

Received March 15, 1994; Revised Manuscript Received May 25, 1995[⊗]

ABSTRACT: The dynamics of phase separation after a temperature jump from the one phase region into the two phase region has been studied on blends of polystyrene (PS) and poly(methyl methacrylate-*stat*-cyclohexyl methacrylate) (PMsC) on different substrates. This system shows a lower critical solution temperature (LCST). The phase separation process followed the mechanism of spinodal decomposition, and the early and late stages could be resolved by using small angle light scattering (SALS). While the early stage could be described by the theory of Cahn and Hilliard, the time dependence of the scattering during the later stages of demixing could be described by power laws. From deviations of Porod's law the interface thickness between two phases was estimated and a new scaling function was proposed.

1. Introduction

Most of the technical polymer blends are multiphase systems, and their properties depend very much on the morphology. Since the morphology is controlled by the way of preparation, it is essential to know the influence of all parameters in the process leading to the phase-separated product. Besides other ways to induce phase transitions, like by shear stresses or pressure jumps, temperature jumps are a convenient and therefore probably the most important way to induce changes in the morphology of a given system. Two different kinds of phase separation are known. Between the coexistence curve and the spinodal curve mixtures are metastable and phase separation starts after exceeding a certain amplitude of concentration fluctuation to form a nucleus of the second phase which grows afterward. This so-called nucleation and growth mechanism leads to irregular-shaped morphologies. The other kind of phase separation is observed inside the spinodal curve (i.e. the unstable region) and is called spinodal decomposition (SD). Here no activation energy barrier has to be overcome by the system and phase separation proceeds in a way that the concentration fluctuations increase mainly on a certain length scale (wavelength). This length scale determines the properties of the system and increases with time. As a result of spinodal decomposition, domains with a smaller size distribution are obtained. For this reason much work has been done on spinodal decomposition after temperature jumps from the one- into the two-phase region. However, if the process of phase separation is not quenched at some time, both kinds of phase separation yield the same macroscopically demixed sample. For example vitrification or cross-linking may stabilize the morphology.

Spinodal decomposition of polymer blends has been extensively investigated by experiments,[1–15] theories,[16–19] and computer simulations.[20–22]

According to Hashimoto et al.[8,10,23] and Cummings et al.[24] different stages of the spinodal decomposition process of a polymer blend can be distinguished: (1) in the early stage only the amplitude of the fluctuation grows but the wavelength remains constant; (2) during the intermediate stage both the wavelength and amplitude change; (3) in the transition stage or late stage 1 the amplitude reaches the equilibrium value but the domains as well as the interface profile are still developing; (4) in the final stage or late stage 2 only a domain growth is observable.

While most of the work so far has been done with rather thick samples (in the range of 100 μm), in this study we use samples with a thickness of only a few micrometers. In this contribution we investigate the influence of the substrate on spinodal decomposition. For that purpose we studied blends of polystyrene (PS) and poly(methyl methacrylate-*stat*-cyclohexyl methacrylate) (PMsC), because the refractive index n of both components differs strongly ($\Delta n = 0.1$) and so enough contrast is given for studies of thin samples. Nishimoto et al.[25] showed that systems of PS and PMsC with different amounts of MMA exhibit a miscibility gap with a lower critical solution temperature (LCST) in an appropriate temperature range for the small angle light scattering (SALS) experiments. In a previous paper[26] we reported about scattering at very small angles occurring at times after a temperature jump into the two-phase region before a spinodal peak shows up. This "anomalous" scattering was interpreted in terms of the Debye-Bueche theory,[27] and an average correlation length smaller than the dominating fluctuation wavelength of the early stage was found. Since that correlation length is related to a random two phase structure, it seems to be connected with another process, the nature of which is not clear yet. Two characteristic times t_1 and t_2 could be found. The spinodal peak appeared at t_2 for the first time. In the present paper we investigate the spinodal decomposition process itself on different substrates and confine ourselves to times larger than t_2.

This paper is divided into the following parts. In section 2 the characterization of the polymers, the preparation of the blends, and a description of the experimental setups are given. Section 3 deals with the theories we use to analyze the early and late stages of SD. The results are presented and discussed in section 4, and our conclusions are given in section 5.

2. Experimental Section

2.1. Sample Preparation. PS was synthesized via anionic polymerization and was obtained from Polymer Standard Service, Mainz, Germany. PMsC was obtained from the

[⊗] Abstract published in *Advance ACS Abstracts,* August 1, 1995.

0024-9297/95/2228-6219$09.00/0

Table 1. Chemical Structure of Poly(methyl methacrylate-*stat*-cyclohexyl methacrylate) (PMsC) and Polystyrene (PS)

	PMsC	PS
molecular structure	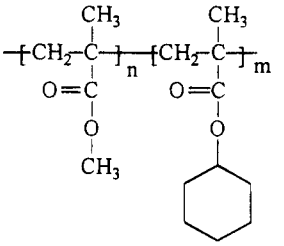	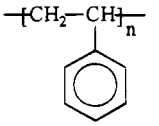
mass of monomer units	MMA: m_0 = 100 g/mol CHMA: m_0 = 168 g/mol	S: m_0 = 104 g/mol

Table 2. Physical Characterization PS and PMsC

	$n_{MMA}(\%)^a$ from elemental analysis	$n_{MMA}(\%)^a$ from ^{1}H-NMR	$\bar{M}_w$ (kg/mol)	$M_w/M_n{}^b$	N_{av}	$T_G{}^c$ (°C)	density ϱ (g/cm^3)	$n_D^{20}{}^d$
PMsC[e]	72	74	116[f]	1.6	977	120	1.14	1.50
PS[g]			270[h]	1.03	2596	100	1.05	1.59

[a] Mole fraction of methyl methacrylate. [b] Ratio of mass-average to number-average molar masses from gel permeation chromatography (GPC). [c] Glass transition temperature from differential scanning calorimetry (DSC). [d] Refractive index of sodium D line at 20 °C. The value for PMsC is a weighted average of the corresponding refractive indices of poly(methyl methacrylate) and poly(cyclohexyl methacrylate). [e] PMsC (synthesized via radical copolymerization with an amount of 73 mol % MMA) was obtained from Deutsches Kunststoff Institut (DKI) in Darmstadt, FRG. [f] Mass-average molar mass from GPC (solvent: tetrahydrofuran; standard: poly(methyl methacrylate); temperature: 20 °C). [g] PS (synthesized via anionic polymerization) was obtained from Polymer Standard Service, Mainz, FRG. [h] Mass-average molar mass from GPC (solvent: tetrahydrofuran; standard: polystyrene; temperature: 20 °C).

Deutsches Kunststoff Institut (DKI) in Darmstadt, Germany, and was prepared by free radical polymerization with an amount of 73 mol % MMA (composition obtained from elemental analysis and ^{1}H-NMR). Tables 1 and 2 show the characteristics of the polymers used in this study.

Thin films, with thicknesses in the range 2−8 μm, were prepared by casting from 1.5 wt % solutions in benzene on a 10 × 20 cm glass plate. After evaporation of the solvent the films were further dried in a vacuum oven at T = 80 °C for 1 day. After cooling to room temperature, the films were cut into pieces with a size of ≈1 cm^2 and were picked up with small, thin glass plates (d = 150 μm) used as carriers on the hotstage. These glass plates were coated with different substrates (gold, carbon) or left unmodified. The samples were dried again for 1 week at about the glass transition temperature at T ≈120 °C under vacuum to relax the preparation stress.

Surface modification of the small glass plates was performed in a vacuum coater (Balzers Union BAE 250). A small amount of the substrate material was evaporated to create a layer of not more than 10 nm (gold) or 50 nm (carbon) thickness. In the case of the gold substrate a 1 nm layer of chromium was deposited first to avoid the formation of islands. These samples show a transparency for λ = 632.8 nm (He−Ne laser) of 50−60%.

2.2. Time-Resolved Small Angle Light Scattering. The principle of a time-resolved small angle light scattering apparatus was described in some earlier papers.[2,28] Figure 1 shows the setup of our SALS apparatus. The incident beam (25 mW He−Ne laser) passes through some apertures to eliminate parasitic scattering. The light is then focused onto the sample by a lens (f = 600 mm). The scattered light coming from the sample falls onto an opaque screen (Marata screen from Spindler & Hoyer, d = 380 mm, distance to the sample 100 mm) to give a scattering pattern which is detected by a low level light CCD-video camera. To increase the intensity range (for the high scattering intensity during the later stages), the camera aperture was reduced during the measurements. After digitizing on an ELTEC E6 68030 minicomputer, online circular averaging of the radial symmetric pattern with a minimum time slice of 4 s reduces the amount of data from 280 kbyte to 2 kbyte.

The transmitted light beam is reflected onto a photodiode by a small mirror to monitor the transmission. The data of the photodiode is read out by a digital multimeter connected via an IEEE 488-bus to the computer. The image intensity is analytically corrected for refraction, double scattering using the transmission data,[29] and geometric effects (projection of a sphere onto a flat screen).[30] Although all of these corrections are small, they sum to an intensity correction factor of about 7 for $\theta \approx 60°$. No corrections were made for camera vignetting, beam shift through cover glasses, scattering volume, and polarization effects due to dipol radiation. If Mie theory for spheres with diameters >1 μm is assumed, the intensity distribution of the different polarization states is neary equal up to θ = 60°.[31] Contributions from further parasitic light, thermal fluctuations, and dark current were collected together in a way that the scattered light obtained immediately after the temperature jump was subtracted as a background from the measured intensity at later times.[24] Due to the optical properties of the opaque screen, the shape of the scattering curves is correct for scattering vectors $q \lesssim 3.5\ \mu m^{-1}$, but the relative change of intensities with time is correct for all scattering vectors.

For determination of cloud point curves the intensity was detected by a single photodiode at a scattering angle of 45° without using the opaque screen.

The temperature jump to the final temperature was done on a microscope hotstage (Linkam THM 600) with a heating rate of 99 °C/min, after the sample had been annealed at a temperature below the cloud point temperature. Despite the high heating rate the electronic controller avoids overheating after reaching the new setpoint. The accuracy of the temperature control is on the order of ±0.2 deg.

2.3. Optical Microscopy. Optical micrographs were taken by a Zeiss microscope and were recorded with the same CCD camera (without objective) as used for the SALS experiments. The sample was placed on the same hostage as used for the SALS experiments. The pictures were digitized and saved on a mass storage. Image processing was performed on a DEC 5000/240 workstation with the PV-Wave software.

3. Theoretical Background

3.1. Early Stage of SD. The early stage of SD is characterized by two features: (1) a maximum with a time independent position $q_m(t = 0)$ appears in the scattering curve (scattering intensity I versus scattering vector q), and (2) the intensity for a given q changes exponentially with time. For deep temperature jumps into the spinodal region contributions to the scattering by thermal noise[16,32] are negligible and the theory of *Cahn* can be used to describe the time evolution of the

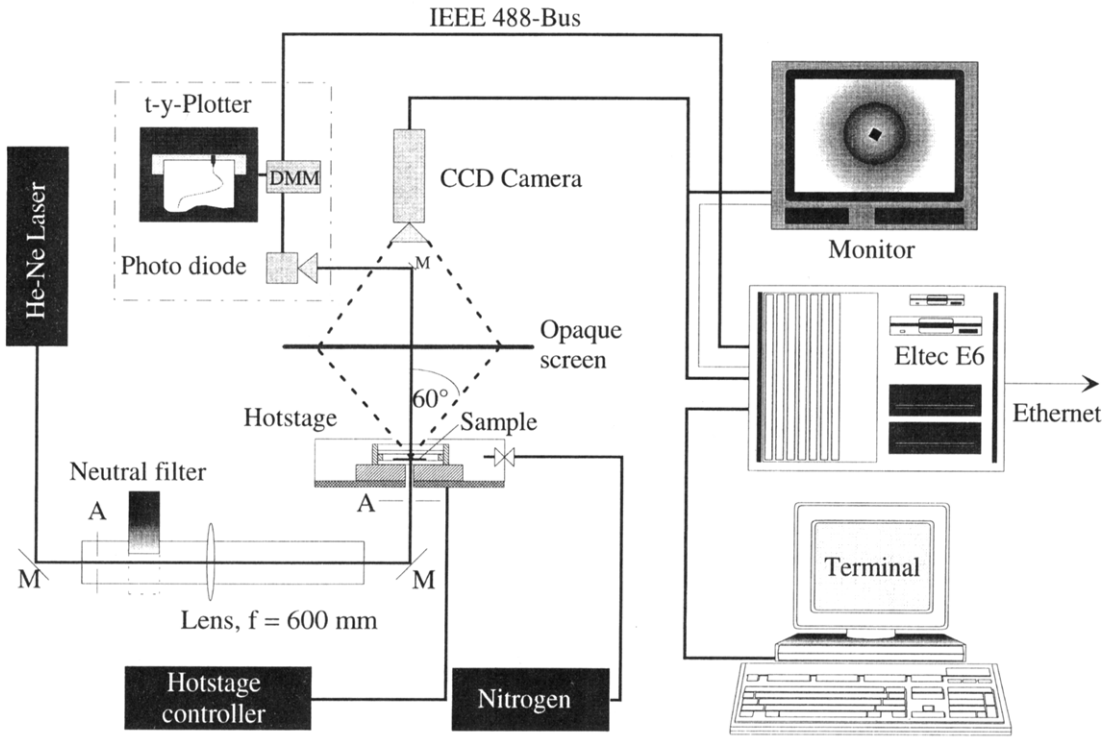

Figure 1. Experimental setup of the SALS apparatus: M, mirror; A, aperture, DMM, digital multimeter.

scattering curve:[33,34]

$$I(q,t) = I(q,0)\exp(2R(q)t) \tag{1}$$

with

$$R(q) = -Mq^2\left(\frac{\partial^2 f_m}{\partial\phi^2} + 2\kappa q^2\right) \tag{2}$$

$R(q)$ is the amplification factor, M is the mobility (assumed to be q-independent), ϕ is the volume fraction of component B, κ is the gradient energy coefficient, f_m is the mean field free energy of mixing, $q = 4\pi/\lambda \sin(\theta/2)$ is the scattering vector with λ being the wavelength of the laser in the sample and θ being the scattering angle, and t is the time.

This approach is limited to concentration fluctuations $\delta\phi$ with small amplitudes $\langle(\delta\phi)^2\rangle \ll (\phi'_{Bin} - \phi''_{Bin})^2$, ϕ'_{Bin}, ϕ''_{Bin} being the compositions on the binodal (coexistence line). According to this theory the structure function shows an exponential increase with time for $q < q_c$ (q_c: critical scattering vector) and an exponential decrease for $q > q_c$.

Equation 2 contains the so-called apparent diffusion coefficient D_{app}, which describes the uphill diffusion during spinodal decomposition:

$$D_{app} = -M\frac{\partial^2 f_m}{\partial\phi^2} \tag{3}$$

Using the random phase approximation[17] to depict the behavior of polymers, the gradient energy coefficient can be expressed by $\kappa = (\langle R^2_{g,A}\rangle N_B + \langle R^2_{g,B}\rangle N_A)/(12(\phi N_B + (1-\phi)N_A))$ where $R_{g,I}$ is the radius of gyration of component I (=A, B) and N_I is the degree of polymerization of component I. $\partial^2 f_m/\partial\phi^2$ can be expressed in terms of the Flory–Huggins theory ($\partial^2 f_m/\partial\phi^2 = 2(\chi_s - \chi)$, where f_m is the Flory–Huggins free energy of mixing, χ is the segmental interaction parameter, and χ_s is the segmental interaction parameter at the spinodal).

From eq 1 it follows that a plot of $\ln(I(q,t))$ versus t yields $R(q)$ and from eqs 2 and 3 it follows that a plot of $R(q)/q^2$ versus q^2 yields mobility from the slope, if the radii of gyration are known, and the apparent diffusion coefficient as the intercept.

Setting eq 2 to zero yields q_c, and differentiation of eq 2 with respect to q yields $q_m(t=0)$, i.e. the scattering vector corresponding to the correlation length of maximal growth $\xi = 1/q_m(t=0)$, which is no function of time:

$$q_c = \sqrt{2}q_m(t=0) = \sqrt{\frac{D_{app}}{2M\kappa}} = \sqrt{\frac{\chi - \chi_s}{\kappa}} \tag{4}$$

To compare the spinodal decomposition of different temperature jumps or different systems, it is useful to define a reference or critical time t_c which allows for a normalization of the absolute time scale by using t/t_c instead of t. t_c is defined by the time a particle needs to move across a distance of the correlation length:

$$t_c = \frac{1}{D_{app}q_m^2(t=0)} \tag{5}$$

3.2. Scaling Analysis of the Structure Function during the Late Stages of SD. After some time in a SD process the maximum of the scattering curve starts to move toward smaller q; i.e. the domain size $\Lambda(t) = 2\pi/q_m(t)$ increases. In this intermediate stage nonlinear behavior of the time evolution of the structure function becomes important[35] and leads to a crossover from exponential growth to a power law behavior for the enlargement of the amplitudes. There the concentration fluctuations have reached the value equal to the coexistence curve and the phase-separating domains still grow in size in order to reduce the interface between the coexisting phases. This power law behavior char-

acterizes the late stages, and for the growth of $q_m(t)$ and $I(q_m(t))$

$$q_m(t) \propto t^{-\alpha} \tag{6}$$

and

$$I(q_m(t)) \propto t^{\beta} \tag{7}$$

are found experimentally.

Theoretical approaches explaining these power laws are well known.[18,36,37] Furukawa introduced the idea of scaling laws for demixing processes after some initial transient time following a temperature jump, so that only a single length scale is established. All physical quantities should depend on time t only through this length scale which is a measure of the domain size of the morphology. It is defined as the inverse of the scattering vector $q_m(t)$, the time dependent position of the maximum of the scattering intensity $I(q,t)$. Asymptotically, the morphology of the phase separating domains is expected to become self-similar in time. For this case it is useful to define a scaled structure factor $F(x,t)$ in the following way:[38,39]

$$F(x,t) = I(q,t)q_m^d(t) \tag{8}$$

with $x = q/q_m(t)$ and $d = 3$ (for a three-dimensional system). To obtain a time- and temperature independent-scaled structure factor $F(x)$, eq 8 has to be divided by the mean square fluctuation of the scattering contrast $\langle\eta^2(t,T)\rangle$, which can approximated by:

$$\langle\eta^2(t,T)\rangle = \int_{q_1}^{q_2} I(q,t,T)q^2\,dq \tag{9}$$

assuming $I(q< q_1,t,T)$ and $I(q>q_2,t,T)$ to be negligible.

After a time t_0 the amplitude of concentration fluctuations reaches the composition of the coexistence curve, i.e. $(\delta\phi_e)^2 = (\phi'_{Bin} - \phi''_{Bin})^2$, $<\eta^2(t,T)>$ = constant. The system then is in the late stages and eq 8 becomes time-independent: $F(x,t\geq t_0) = F(x)$. Then the relation between the exponents

$$\beta = 3\alpha \tag{10}$$

is valid, while for intermediate and early stages the relation is $\beta > 3\alpha$.

As a proposal to describe the x dependence of $F(x)$ Furukawa introduced the following scaled structure function:[18]

$$F(x) = (1 + \gamma/\nu)\frac{x^{\nu}}{\gamma/\nu + x^{\nu+\gamma}} \tag{11}$$

The parameter ν describes the structure in the low q range, and γ dominates in the high q range.

Some theoretical investigations[19] and computer simulations[40-43] suggest $2 < \nu < 4$, but from light-scattering experiments most often $\nu = 2$ was obtained except for ref 44. The γ parameter depends on the occurrence of curved or noncurved sharp interfaces.[18] If the concentration of the minority phase is below the percolation limit $\phi_p \sim 0.16$,[45] eq 11 yields Porod law behavior with $\gamma = d + 1$ for $\phi < \phi_p$ and $\gamma = 2d$ for $\phi_c > \phi > \phi_p$.

Computer simulations[40-43] and experimental results[8,23,44] near the critical composition ϕ_c of polymer blends and also low molecular systems[46] show strong deviations in the high q range from all kinds of eq 11. Higher order maxima or shoulders in the scattering curves indicate that one length scale may not be enough to characterize the system completely. Also length scales smaller than the average domain size have to be considered, especially at larger x.

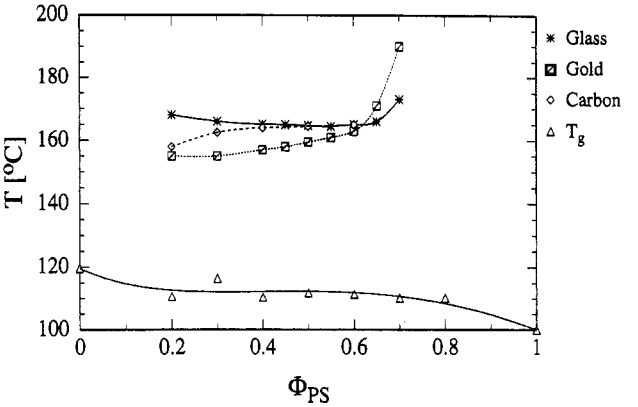

Figure 2. Phase diagrams of thin films (4 μm) of PMsC/PS on different substrates. The points are obtained by extrapolation of at least two cloud points measured with different heating rates, to heating rate zero. The lines between points are cubic splines as a guide to the eyes only. Glass transition temperatures T_g are obtained by differential scanning calorimetry. The line is a guide to the eye only.

Such a smaller length scale could be an average curvature of the interfaces as well as a finite interface thickness.[8] Here we assume the average curvature of the domain interfaces to have a time dependence similar to that of the average domain size, so only the interface thickness is considered to have a different time behavior. An interface profile may be approximated by a tanh function[45,47,48] or a Gaussian profile.[49,50]

Besides others (see for example ref 51), Hashimoto has modified the expression for the scattering intensity in order to account for the deviation from Porod's law by introducing the interface thickness $t_1(t) = (2\pi)^{1/2}\sigma(t)$:[8,10,23]

$$I(q,t) \propto \langle\eta^2\rangle\Sigma(t)q^{-4}\exp[-\sigma(t)^2q^2] \tag{12}$$

with the interface density $\Sigma(t)$. A plot of $\ln(I(q,t)q^4)$ vs q^2 should give a straight line for $x > 1$ and yields the interface thickness from the slope. In the limit of $\sigma \to 0$ for eq 12 Porod's law is obtained.

4. Results and Discussion

4.1. Determination of the Phase Diagrams. The phase diagrams were obtained by heating up samples very slowly for two or three different heating rates from the one-phase region into the two phase region. The temperature where the intensity detected by a photodiode increases strongly was defined as the cloud point temperature. From extrapolation of these cloud points as a function of heating rate to heating rate zero, the equilibrium cloud point was obtained. The uncertainty of this temperature is on the order of 2 deg. Figure 2 shows the phase diagrams obtained on glass, gold, and carbon substrates. It can be seen that the samples with a low PS content are more stable on glass than on the gold substrate. Compositions with a higher amount of PS exhibit a lower phase separation temperature on glass. Light-scattering results are presented only for compositions of ϕ_{PS} of 0.5 and 0.4 because of the most contrast and best film quality compared with other compositions. Smaller compositions have poor contrast,

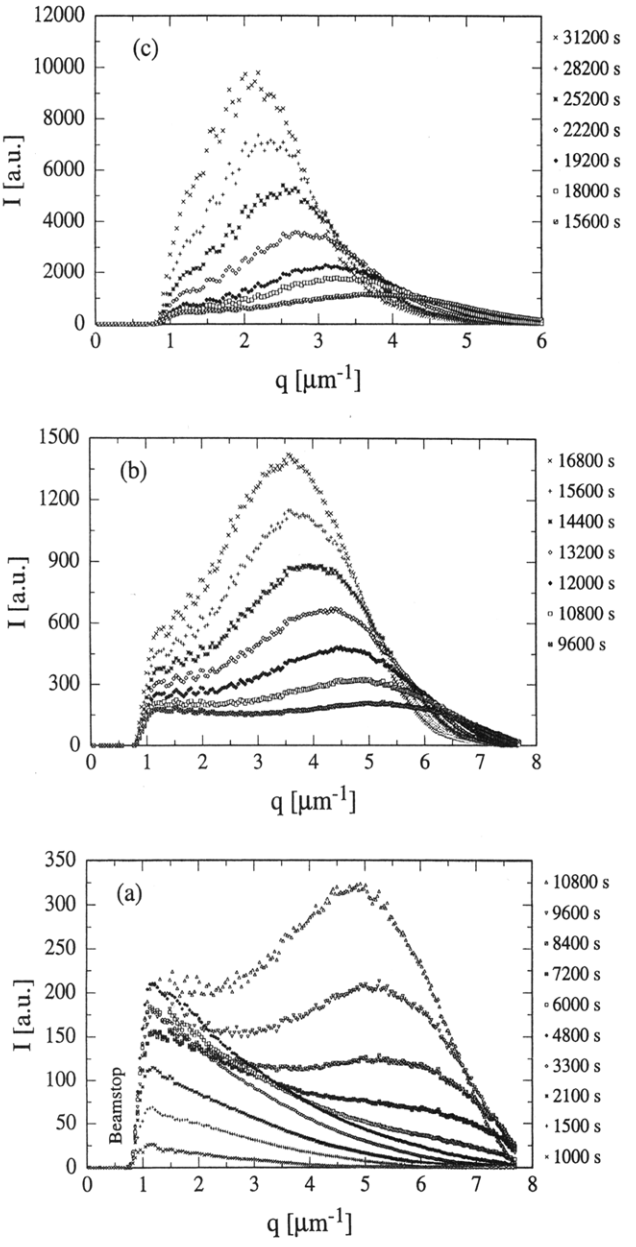

Figure 3. For a sample of composition $\phi_{PS} = 0.5$ prepared on unmodified glass substrate a temperature jump to 185 °C was made after annealing at 150 °C. Evolution of the intensity versus q was recorded for the early (a), intermediate (b), and late stage (c).

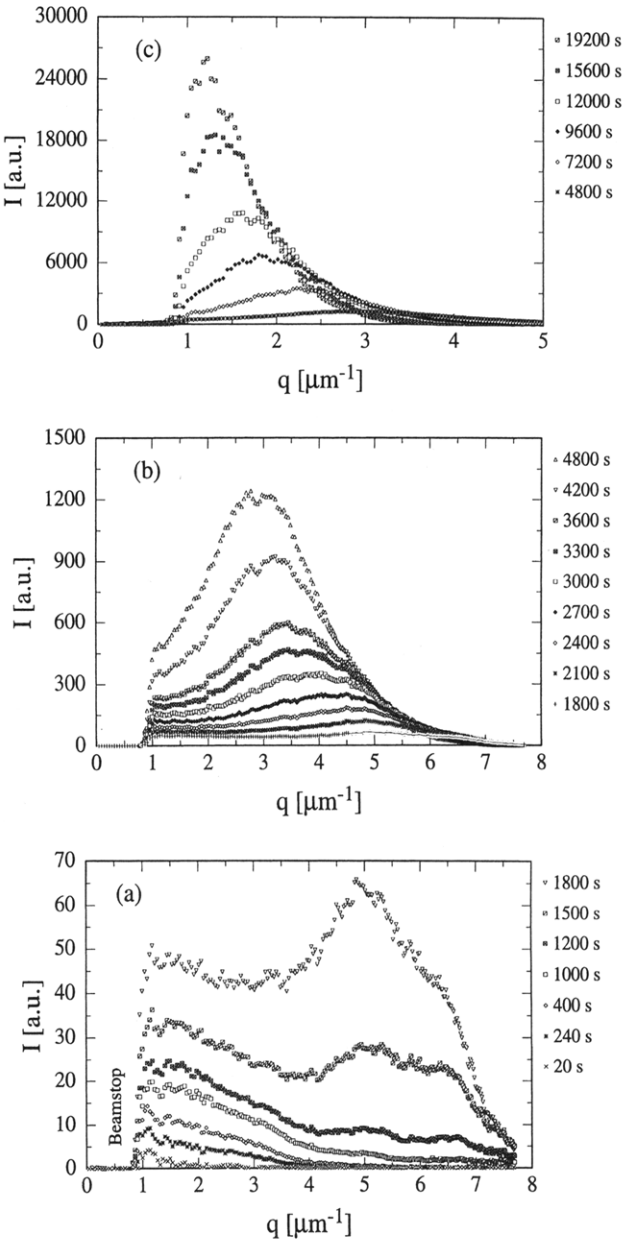

Figure 4. For a sample of composition $\phi_{PS} = 0.5$ prepared on gold substrate a temperature jump to 185 °C was made after annealing at 135 °C. Evolution of the intensity versus q was recorded for the early (a), intermediate (b), and late stage (c).

and the larger one developed large scale inhomogeneities (millimeter range) during the casting process. This gives at the beginning of the investigations the first indication of a strong surface effect on the phase behavior of thin films of the PS/PMsC system.

From the work of Reich and Cohen[52] a substrate effect for thin polymer films on the phase separation temperature is well-known. They proposed two kinds of interaction between the polymer film and the substrate which destabilize the mixture: a selective adsorption of one of the components or electrostatic interaction with the charged glass surface as well as a pure geometric effect which leads to a decrease of contacts between different polymer segments near the surface. This would lead to different phase diagrams for different substrates.

4.2. Time evolution of scattering profiles during the early stage of SD. After annealing the sample for 1 h between the cloud point and T_g at $T = 150$ °C, temperature jumps into the two-phase region were done. Figures 3 and 4 show the evolution of the scattering curves with time for temperature jumps to $T = 185$ °C on glass and gold substrates, respectively. The results obtained from experiments using a carbon substrate are similar to the results on gold substrate and are not further discussed.

Because the anomalous scattering intensity for experiments on the gold substrate is much weaker than that on the glass substrate, an analysis according to the Cahn–Hilliard theory could be done for experiments on the gold substrate only. The growth of structures is faster on gold than on the glass substrate. This can be understood by considering the deeper jump into the two-phase region (see Figure 2).

The double peak structure in Figure 4a with developing maxima at $q_{m,1} = 5$ and $q_{m,2} = 6.5$ μm^{-1} does not perturbate the Cahn–Hilliard analysis. Both peaks do not change their position over a wide time range, but

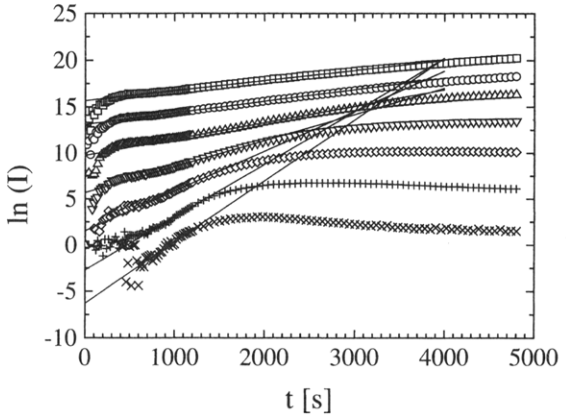

Figure 5. Semilogarithmic plot of the scattering intensities versus time of the sample of Figure 4 during the early stages of SD for different q values. (□) 1.58; (○) 2.01; (△) 3.01; (▽) 4.01; (◇) 5.01; (+) 6.00; (×) 7.00 μm^{-1}.

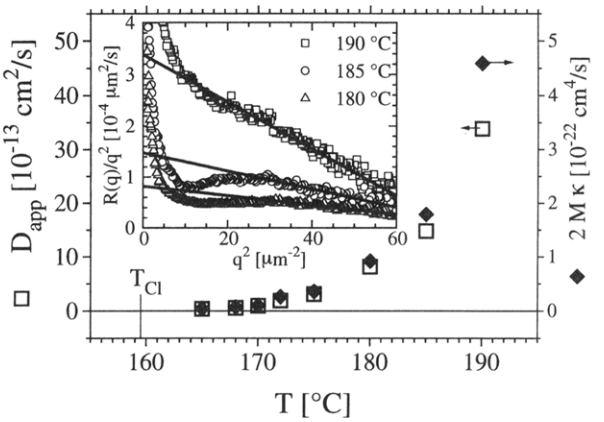

Figure 6. Temperature dependence of the apparent diffusion coefficient and the product of collective mobility and gradient energy coefficient, as obtained from the intercept and slope of the plots of $R(q)/q^2$ versus q^2 (inlay), respectively.

the peak at $q_{m,1}$ grows more rapidly than the other for longer times. The peak at $q_{m,2}$ remains only as a shoulder of the bigger one (see also in ref 13). The peak at $q_{m,2}$ is the peak which the Cahn–Hilliard analysis predicts. The development of multiple peaks during phase separation was also observed by *Han* et al. for a system of poly(styrene-*stat*-*p*-(1,1,1,3,3,3-hexafluoro-2-hydroxyisopropyl)-α-styrene) and poly(butyl methacrylate).[11] They explained their data with rather broad polydispersities of the polymer components as well as heterogeneities in the sequence statistics of the copolymer, which may lead to a simultaneous phase separation into multiple systems; another explanation is the possible existence of small local inhomogeneities induced by the preparation of the blends by solution casting.

The experiments on the glass substrate do not show any double peak, this occurs only on gold and carbon substrates! It might be that the high intensity of the anomalous scattering during the early stage covers one of the double peaks.

The semilogarithmic plot of the intensity evolution of various q values versus time (Figure 5) yields from the initial slopes a q-dependent amplification factor (eq 2). In this plot one can see the influence of anomalous scattering at the lower scattering angles. We suppose that the analysis of Figure 5 is nevertheless correct, because linearity of $\ln(I)$ versus t is obtained over a wide range of time. The larger the q values, the earlier a deviation from an exponential increase of the intensity occurs, which is a consequence of the coarsening process of the spinodal structure.

The inlay of Figure 6 shows some results of the Cahn–Hilliard plot. For different temperature jumps a fairly good linear relationship at large q is obtained, indicating that this stage of spinodal decomposition can be well described by this theory. From the intercepts of such plots a temperature dependent apparent diffusion coefficient (eq 3) and the slope the q value of the dominating concentration fluctuation (eq 4) are obtained. The latter can be used for a consistency check of the scattering data, because it should be similar to the experimental q value, where a scattering maximum appears for the first time. The agreement is good, as shown in Table 3.

It is important to note that $q_m(t=0,T)$ does not change in this temperature range. Also from other investigations on rather thin films such a behavior is known.[12,15]

A plot of D_{app} and the product $M\kappa$ as a function of temperature shows nearly exponential behavior in the investigated temperature range (Figure 6). According to eq 4 this means a very weak temperature dependence of $(\chi - \chi_s)$. One can assume that near T_s a stronger T dependence should occur; otherwise no spinodal could exist. Evidently, the approximations are not good enough to describe the expected temperature dependence of $q_m(t=0,T)$. No critical slowing down near the spinodal temperature is observed, because the experiments may have been done too far away from the spinodal temperature. In this case the temperature dependence of D_{app} is approximately the same as for M and a determination of the spinodal temperature T_s by extrapolation of D_{app} to zero is impossible. This means, further, that the experiments were carried out in the diffusion controlled regime. The results of the Cahn–Hilliard analysis are given in Table 3.

From the Arrhenius-like temperature dependence of the collective mobility M (Figure 7) a rather high activation energy of $E_A = 231$ kJ/mol is obtained. This is comparable to a value of 268 kJ/mol for the similar system PS/PCHMA, as obtained by fluorescence microdensitometry.[53]

4.3. Test of Furukawa's Scaling Postulate for the Domain Growth. For the later stages (Figures 3b,c and 4b,c) the peak position of the scattering profiles

Table 3. Characteristic Parameters Describing the Early Stage of Spinodal Decomposition

T (°C)	$2D_{app}$ (10^{-13} cm^2/s)	$4M\kappa$ (10^{-22} cm^4/s)	$q_m(t=0)$ (μm^{-1}) (eq 4)	$q_m(t=0)$ (μm^{-1}) (experiment)	t_c (s) (eq 5)
165	0.773	0.0875	6.65	6.4	5851
168	1.122	0.147	6.18	6.5	4661
170	1.935	0.200	6.95	6.9	2138
172	3.826	0.530	6.01	6.7	1449
175	6.241	0.718	6.59	6.5	736.9
180	16.36	1.839	6.67	6.3	274.7
185	29.55	3.577	6.43	6.5	163.9
190	67.70	9.178	6.07	6.0	80.09

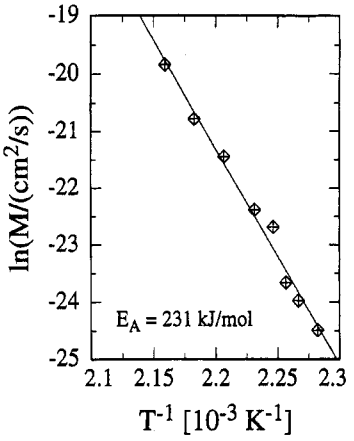

Figure 7. Arrhenius plot of the collective mobility (data from Figure 6).

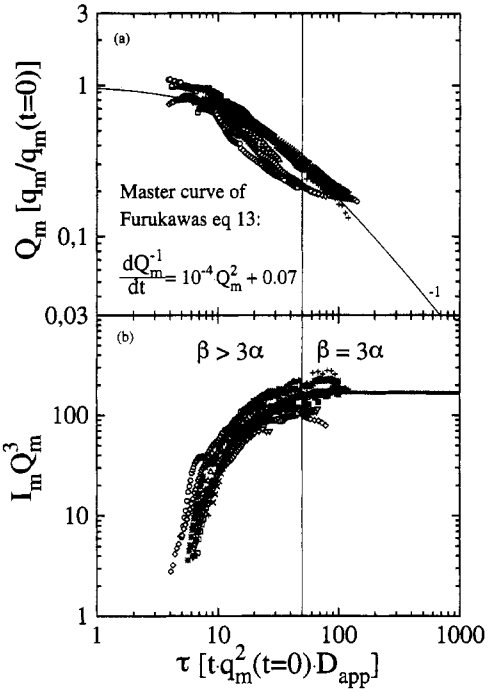

Figure 8. (a) The reduced wavenumber Q_m plotted as a function of the reduced time τ for eight different temperatures. The solid line is a fit of eq 13 using a numerical solution by the Runge–Kutta scheme.[54] (b) Plot of $I_mQ_m^3$ vs τ for testing the relation $\beta = 3\alpha$ for the late stage of phase separation. (□) 165 °C; (○) 168 °C; (△) 170 °C; (▽) 172 °C; (◇) 175 °C; (+) 180 °C; (×) 185 °C; (*) 190 °C; (⊠) 190 °C.

shifts to smaller wavenumbers while the intensity increases with time, indicating the growth both of amplitude and wavelength of the fluctuation. Qualitatively, the scattering curves during the later stages are similar for both substrates.

A plot of the reduced wave number $Q_m = q_m(t)/q_m(t=0)$ of the maximum position versus the reduced time $\tau = t/t_c$ (Figure 8a) can be described by the equation for the time dependence of Q_m for a liquid derived by Furukawa:[18]

$$\frac{\partial Q_m^{-1}}{\partial \tau} = AQ_m^{\,2} + B \qquad A, B \neq 0 \tag{13}$$

with A and B being related to the mobility and free energy of the system. In the long time limit is $Q_m \propto \tau^{-1}$. This function shows the behavior of a liquid entering the final stage (hydrodynamic flow), but the predicted limit of the exponent $\alpha = 1$ was not reached. The maximum was at $\alpha \approx 0.8$ for the long time behavior of phase separation. From a plot of $I_m(\tau)Q_m^3(\tau)$ vs τ (Figure 8b) there is an indication that despite the thin film geometry a three-dimensional growth of the domains happens in the sample, because a plateau is reached for reduced times $\tau > \tau_0 \approx 50$. A plot of $I_m(\tau)Q_m^2(\tau)$ vs τ, describing a pure two-dimensional growth, does not show a plateau in the investigated time range.

4.4. Influence of the Substrate on Domain Growth. An Analysis of Optical Micrographs. The strong influence of the substrate on the domain growth during the late stage of SD can be seen in the optical micrographs (Figure 9 a–c). For this experiment the glass substrate was only partially modified with a gold layer (~10 nm). A thin polymer blend film with a composition of $\phi_{PS} = 0.4$ deposited on the partially modified substrate then was heated to $T = 200$ °C. A sharp interface line in the middle of each picture marks the border between the two different substrates. The average distance between similar structures was used as a measure of the correlation length, and a corresponding wavenumber could be obtained. Figure 10 shows the time evolution of that wavenumber for the experiments on both substrates, and an exponent similar to the results from SALS is found. The faster domain growth on gold than on the glass substrate comes from a deeper temperature jump inside the two-phase region. This is in agreement with the substrate dependence of the cloud point curves.

4.5 Time Evolution of Scattering Profiles during the Later Stages of SD. As pointed out in section 3.2 the scaled intensity should match a single master curve if only one time-dependent length parameter describes the growth of the structure. Figure 11a presents the data of the scaled structure function $F(x)$ in the late stage for reduced times $\tau > \tau_0 \approx 50$. The early and intermediate stages in this representation are similar to the results of Hashimoto et al.[8] and are not shown here for the sake of clarity. Universal behavior is obtained only for $F(x,t)$ at $x \approx 1$. This implies that only the global structure in the range of $q \cong q_m(t)$ scales with a single length parameter $\Lambda(t)$. For $x > 1.5$ one can observe further growing until for times $\tau > 100$ a stationary state for all x is obtained. This indicates structural changes on smaller length scales which are not following the time dependence of $\Lambda(t)$.

The time interval $50 < \tau < 100$ we define in accordance to the work of Hashimoto et al.[8,23] as late stage 1, and as late stage 2 is the region where the system is self-similar all over the accessible q range.

Since the experiments were performed with samples of $\phi_{PS} = 0.5$, which is not far away from the critical concentration of $\phi_{c,PS} \approx 0.39$ (calculated under the assumption of a concentration independent χ parameter), for a three-dimensional system ($d = 3$) we should yield an exponent of $n = -6$ for the scaled structure function

$$F(x) \propto x^n \tag{14}$$

in the higher q range.

Our results give power law dependence's other than expected. For $1.5 < x < 2.5$ the decrease of the intensity goes with $n = -4$, as described by *Furukawa* for nonpercolated structures. The decrease of the intensity for the higher wavenumbers is much stronger with

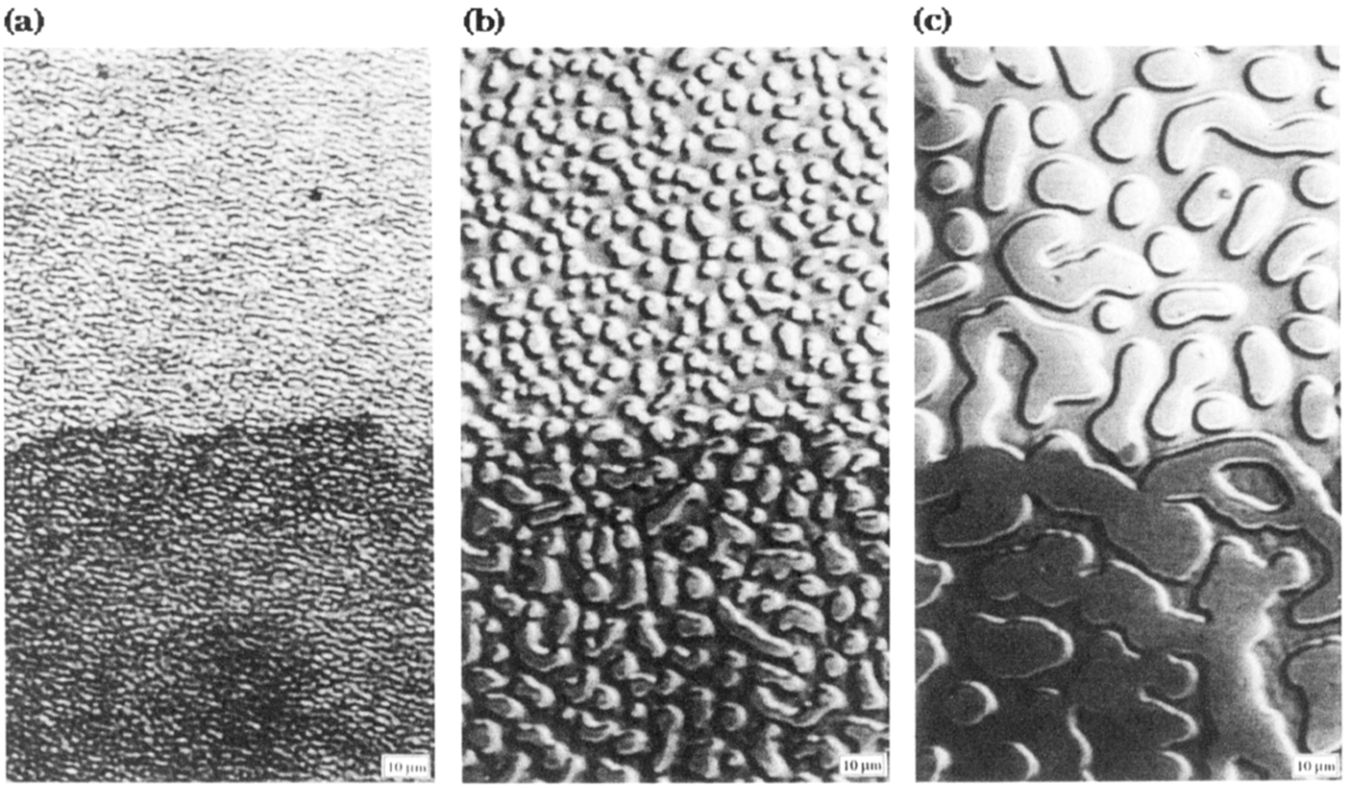

Figure 9. Digitized microscope pictures presenting the structure evolution of a sample with $\phi_{PS} = 0.4$ after a temperature jump from 135 to 200 °C simultaneously on glass substrate and gold substrate. The upper part belongs to the domains on the highly transparent unmodified glass, and the lower part belongs to the structures on the less transparent gold layer. A typical spinodal structure with an average wavelength of about 1 μm is visible in (a). A droplet structure occurs in (b) showing structures of the size of the film thickness. The structures on glass are smaller than on the gold-modified surface. This difference becomes larger for long times (c). The domain size differs by a factor of approximately $^1/_3$.

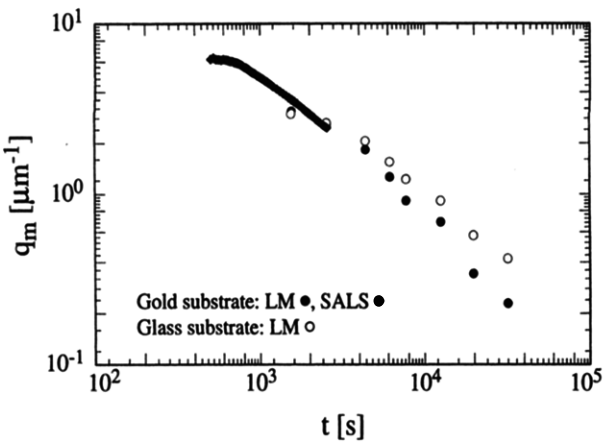

Figure 10. Representation of the structure evoluton of the data obtained by light microscopy (Figure 9) in the q space. (●) gold substrate, (○) glass substrate. For comparison also included are the date for gold substrate from SALS (◆).

exponents in the range from $n = -12$ to $n = -8$. For $x < 1$ an exponent of $n = 2$ was found.

For the deviation at $x > 2.5$ we have to take into account the scattering of structures with a smaller length scale than the average droplet radius. This could be an average curvature of the interfaces as well as a finite interface thickness. Because of the small irregularity of the droplet shape (Figure 9b,c) we focus our attention on the change of the interface profile with time.

A fit of eq 12 to our data (Figure 12) yields for a plot of $I(q,t)q^4$ vs q^2 a straight line with a slightly increasing slope with time. Since the slope is proportional to the square of the interface thickness t_I, this means that the interface thickness increases with time. This behavior was confirmed also for other temperatures (Figure 13).

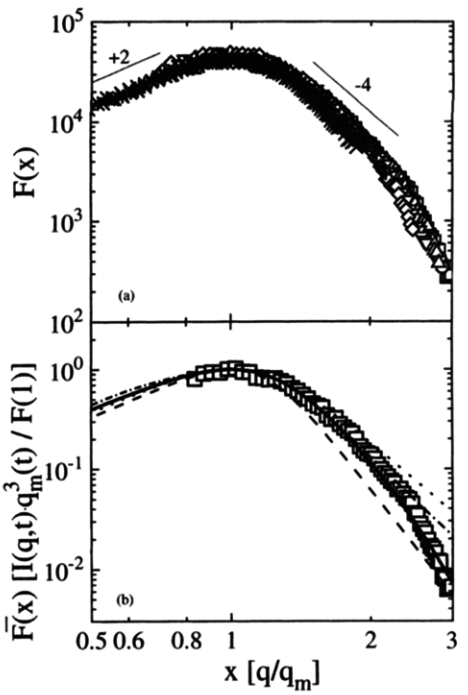

Figure 11. (a) Double logarithmic plot of the scaled intensity $F(x)$ in the late stage of phase separation with the data from Figure 4c. (□) 19 200 s, $\tau = 117.1$; (○) 18 720 s; (△) 17 760 s; (▽) 16 800 s; (◇) 14 880 s; (+) 12 000 s; (×) 9600 s; (*) 8640 s, $\tau = 52.7$. (b) Normalized scaling function $F(x)/F(1)$ for $t =$ 19 200 s ($\tau = 117.1$) (□) with miscellaneous theoretical scaling functions: (—) $\bar{F} \propto x^2/(B + x^6)\exp(-\tilde{\sigma}^2x^2)$; (— · —) Fratzl and Lebowitz;[51] (· · ·) $\bar{F} \propto x^2/(2 + x^6)$; (— — —) $\bar{F} \propto x^2/(2 + x^8)$.

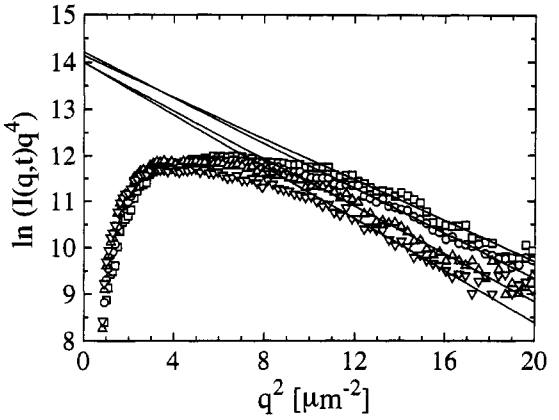

Figure 12. Plots of $\ln(I(q,t)q^4)$ vs q^2 for evaluating the interface thickness. (□) 5100 s, $\tau = 63.8$; (○) 6000 s; (△) 6900 s; (▽) 7800 s, $\tau = 97.5$.

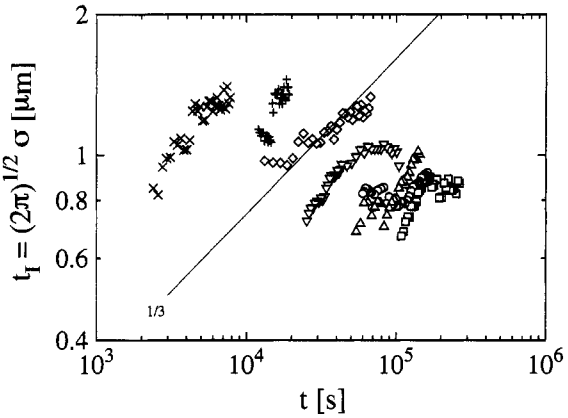

Figure 13. Plots of the time evolution of the interface thickness for different temperatures. The straight line is only a suggestion for a power grow law like $t_I \propto t^{1/3}$. (□) 165 °C; (○) 168 °C; (△) 170 °C; (▽) 175 °C; (◇) 180 °C; (+) 185 °C; (×) 190 °C.

Since the copolymer in our samples might have a distribution in composition besides its polydispersity, an increasing interface thickness could be caused by a fractionation perpendicular to the domain boundaries with respect to both molecular weight and composition, which follows different time dependences.

For the later times a constant value of the interface thickness t_I was obtained. This confirms that the time dependence of the structure is then given by the time dependence of only one length scale; i.e. the system has reached late stage 2.

A test of different scaling functions is shown in Figure 11b. None of the cited scaling functions from Furukawa[18] or Fratzl and Lebowitz[51] show for the whole q range a satisfactory accordance with our measured data. For that reason a new scaling function was suggested by a compilation of Furukawa's and Hashimoto's functions, eqs 11 and 12. After normalization we get with $F(1) \equiv 1$ a description for the scaling function with a finite interface thickness of a Gaussian profile:

$$F(x) = (B + 1)\exp(\tilde{\sigma}^2)\frac{x^2}{B + x^6}\exp(-\tilde{\sigma}^2 x^2) \quad (15)$$

$B = 3/(1 - \tilde{\sigma}^2) - 1$, and the scaled interface thickness is $\tilde{\sigma} = \sigma(t)q_m(t)$.

The thickness $t_1 = (2\pi)^{1/2}\sigma$ calculated by these fits gives the same results as eq 12.

5. Conclusion

Cloud point curves of the blend PS/PMsC have been measured using different substrates. The blends are of the LCST type, and the cloud point temperatures are influenced by the substrate. The phase separation dynamics after temperature jumps into the instability region of the phase diagram shows deviations from the behavior reported for many other systems. After an initial scattering at small angles which can be characterized by a correlation length of a random two phase structure, the growing of structures on the gold substrate can be well described by the linear Cahn–Hilliard theory, although a double-peak structure is observed. The wavelength of the most growing fluctuation was found to be almost independent of temperature. This means a very weak dependence of the Flory–Huggins χ parameter on the temperature, as well as an exponential temperature dependence of the apparent diffusion coefficient. The later stages of SD can be described by scaling laws, which take into account the different time dependence of the interface thickness between the growing domains and the size of the domains themselves. A full description of the scaled structure factor is possible by a combination of Furukawa's scaling function, which considers the system's dependence on the size or average distance of the domains only, and a scaling function describing the deviations from Porod's law at large scattering vectors.

Acknowledgment. I thank Prof. Dr. E. W. Fischer for helpful discussions and Dr. G. P. Hellmann from the Deutsches Kunststoff Institut in Darmstadt for the copolymer. I would also like to thank Dr. U. Fasting and Dr. W. Theobald for their technical assistance during preparation of the manuscript. This work was mainly supported by the Bundesministerium für Wirtschaft (AiF-project No. 7695).

References and Notes

(1) Bruder, F.; Brenn, R. *Phys. Rev. Lett.* **1992**, *69*, 624.
(2) Hashimoto, T.; Kumaki, J.; Kawai, H. *Macromolecules* **1983**, *16*, 641.
(3) Hashimoto, T.; Itakura, M.; Hasegawa, H. *J. Chem. Phys.* **1986**, *85*, 6118.
(4) Hashimoto, T.; Itakura, M.; Shimidzu, N. *J. Chem. Phys.* **1986**, *85*, 6773.
(5) Hashimoto, T. In *Current Topics in Polymer Science* ; Ottenbrite, R. M., Utracki, L. A., Inoue, T. Eds.; Carl Hanser Verlag: München, 1987; Vol. 2.
(6) Hashimoto, T.; Takenaka, M.; Izumitani, T. *Polym. Commun.* **1989**, *30*, 45.
(7) Hashimoto, T.; Takenaka, M.; Jinnai, H. *Polym. Commun.* **1989**, *30*, 177.
(8) Hashimoto, T.; Takenaka, M.; Jinnai, H. *J. Appl. Crystallogr.* **1991**, *30*, 457.
(9) Hashimoto, T.; Takenaka, M.; Izumitani, T. *J. Phys. Chem.* **1992**, *97*, 678.
(10) Hashimoto, T. In *Structure of Polymer Blends*, Thomas, E. L., Ed.; Material Science and Technology; VCH: Weinheim, 1993; Vol. 12.
(11) He, M.; Liu, Y. Y.; Feng, M.; Yang, C.; Han, C. *Macromolecules.* **1991**, *24*, 464.
(12) Kyu, T.; Saldanha, J. *Macromolecules* **1988**, *21*, 1021.
(13) Lim, D.; Kyu, T. *J. Chem. Phys.* **1990**, *92*, 3944.
(14) Roe, R.-J.; Kuo, C.-M. *Macromolecules* **1990**, *23*, 4635.
(15) Snyder, H. L.; Meakin, P.; Reich, S. *Macromolecules* **1983**, *16*, 757.
(16) Binder, K. *J. Chem. Phys.* **1983**, *79*, 6387.
(17) de Gennes, P. G. *J. Chem. Phys.* **1980**, *72*, 4756.
(18) Furukawa, H. *Adv. Phys.* **1985**, *34*, 703.
(19) Furukawa, H. *Prog. Theor. Phys. Suppl.* **1989**, *99*, 358.
(20) Ball, R. C.; Essery, R. L. H. *J. Phys.: Condens. Matter* **1990**, *2*, 10303.
(21) Chakrabarti, A. *Phys. Rev. Lett.* **1992**, *69*, 1548.

(22) Puri, S.; Binder, K. *Phys. Rev. A* **1992,** *46,* R4487.
(23) Takenaka, M.; Hashimoto, T. *J. Chem. Phys.* **1992,** *96,* 6177.
(24) Cummings, A.; Wilzius, P.; Bates, F. S.; Rosendale, J. H. *Phys. Rev. A* **1992,** *45,* 885.
(25) Nishimoto, M.; Keskkula, H.; Paul, D. *Macromolecules* **1990,** *23,* 3633.
(26) Edel, V.; Abetz, V. *Makromol. Chem., Rapid. Commun.* **1993,** *14,* 753.
(27) Debye, P.; Bueche, A. M. *J. Appl. Phys* **1949,** *20,* 518.
(28) Kyu, T.; Saldanha, J. *J. Polym. Sci., Polym. Lett. Ed.* **1988,** *26,* 33.
(29) Stein, R. S.; Keane, J. J. *J. Polym. Sci.* **1955,** *17,* 21.
(30) Edel, V. *Kleinwinkellichtstreuuntersuchungen zum Entmischungsverhalten von binären Polymermischungen aus Polystyrol und Poly(methylmethacrylat-stat-cyclohexylmethacrylat)*; Verlag Shaker: Aachen, 1993.
(31) van de Hulst, H. C. *Light Scattering by Small Particles*, Dover Publications, Inc.: New York, 1981.
(32) Cook, E. H. *Acta Metall.* **1970,** *18,* 297.
(33) Cahn, J. W. *Trans. Metall. Soc. AIME* **1968,** *242,* 166.
(34) Cahn, J. W. *J. Chem. Phys.* **1965,** *42,* 93.
(35) Langer, J. S.; Bar-on, M.; Miller, H. D. *Phys. Rev. A* **1975,** *11,* 1417.
(36) Binder, K.; Stauffer, D. *Phys. Rev. Lett.* **1974,** *33,* 1006.
(37) Lifshitz, I. M.; Slyozov, V. V. *J. Phys. Chem. Solids* **1961,** *19,* 35.
(38) Binder, K. In *Spinodal Decomposition*; Haasen, P. Ed.; Material Science and Technology; VCH: Weinheim, 1991; Vol. 5.
(39) Gunton, J. D.; San Miguel, M.; Sahni, P. S.; In *Phase Transitions and Critical Phenomena*; Domb, C., Lebowitz, J. L., Eds.; Academic Press: London, 1983; Vol. 8.
(40) Chakrabarti, A.; Toral, R.; Gunton, J. D.; Muthukumar, M. *J. Chem. Phys.* **1990,** *92,* 6899.
(41) Ohta, T.; Nozaki, H. In *Space-Time Organization in Macromolecular Fluids*; Tanaka, F., Doi, M., Ohta, T., Eds.; Springer Series in Chemical Physics Vol. 51, Springer Verlag: Berlin, 1989.
(42) Shinozaki, A.; Oono, Y. *Phys. Rev. Lett.* **1991,** *66,* 173.
(43) Toral, R.; Chakrabarti, A.; Gunton, J. D. *Phys. Rev. Lett.* **1988,** *60,* 2311.
(44) Takenaka, M.; Itzumitiani, T.; Hashimoto, T. *J. Chem. Phys.* **1990,** *92,* 4566.
(45) Tomita, H. In *Statistics and Geometry of Random Interface Systems*; Kawasaki, K., Suzuki, M., Onuki, A., Eds.; Formation, Dynamics and Statistics of Pattern; World Scientific Publishing: Singapore, 1990; Vol. 1.
(46) Kubota, K.; Kuwahara, N.; Eda, H.; Sakazume, M.; Takiwaki, K. *J. Chem. Phys.* **1992,** *97,* 9291.
(47) Cahn, J. W.; Hilliard, J. E. *J. Chem. Phys.* **1958,** *28,* 258.
(48) Joanny, J. F.; Leibler, L. *J. Phys.* **1978,** *39,* 951.
(49) Ruland, W. *Macromolecules* **1987,** *20,* 87.
(50) Stein, R. S. In *Optical Behaviour of Polymer Blends*; Paul, D. R., Newman, S. Eds.; Polymer Blends; Academic Press; New York, 1978; Vol. 1.
(51) Fratzl, R.; Lebowitz, J. L. *Acta Metall.* **1989,** *37,* 3245.
(52) Reich, S.; Cohen, Y. *J. Polym. Sci., Polym. Phys. Ed.* **1981,** *19,* 1255.
(53) Best, M.; Sillescu, H. *Polymer* **1992,** *33,* 5245.
(54) Bronstein, I. N.; Semendjajew, K. A. *Taschenbuch der Mathematik*; Harri Deutsch: Thun, 1987.

MA946343X